LBL--22317

DE87 003525

BRIGHTNESS AND COHERENCE OF SYNCHROTRON RADIATION AND HIGH-GAIN FREE ELECTRON LASERS

Kwang-Je Kim

Center for X-ray Optics
Lawrence Berkeley Laboratory
University of California
Berkeley, CA 94720, USA

Paper presented at the
VII National Conference on
Synchrotron Radiation (SR-86)
Novosibirsk, USSR

June 3–5, 1986

DISCLAIMER

This work is supported by the Office of Basic Energy Sciences of the U.S. Department of Energy under Contract No. DE-AC03-76SF00098

BRIGHTNESS AND COHERENCE OF SYNCHROTRON RADIATION AND HIGH-GAIN FREE ELECTRON LASERS

Abstract

We review the characteristics of synchrotron radiation with particular attention to its phase-space properties and coherence. We also discuss the transition of the simple undulator radiation to more intense, more coherent high-gain free electron lasers.

1. Introduction

Synchrotron radiation devices—bending magnets, wigglers, and undulators—in next-generation, low-emittance electron storage rings are sources of high-brightness radiation in the wide spectral region covering photon energies between several eV and several tens of keV. Furthermore, the undulator radiation from 1 to 2 GeV rings will have substantial coherence properties in the vacuum ultraviolet (VUV) and the soft x-ray regions, generating tens of milliwatts of time-averaged, transversely coherent power of 1-micron coherence length [1]. In this paper we shall summarize the characteristics of synchrotron radiation with particular emphasis on the brightness and the coherence properties. As the number of undulator periods N increases, the cumulative effects of radiation–electron beam interaction can lead to an exponential amplification in radiation intensity [2] and significantly enhanced coherence properties over simple undulator radiation. We shall review the radiation characteristics in this so-called high-gain free electron laser regime.

The angular distribution and the intensity characteristics of synchrotron radiation are extensively reviewed in the literature [3]. To describe how the radiation propagates through free space and lenses, and how it forms images and interference patterns, however, it is necessary to understand the flux distribution in angle-position phase space. The flux density in phase space is called the brightness, which is invariant under optical transformation and therefore a true characterization of the source strength. The photon flux contained in that portion of the phase space whose area is less than the coherent phase-space area, given by $\lambda/2$ where λ is the wavelength, is transversely coherent. For synchrotron radiation, the brightness can be rigorously calculated in terms of the Wigner distribution function [4,5]. Although the resulting formulas are complicated, the important features of the phase space distribution can be understood by suitable approximation. These are the subjects of Sections 2 and 3.

The evolution of radiation characteristics and the electron correlation from simple undulators to high-gain free electron lasers can be determined by solving the Maxwell-Klimontovich equations [6]. The radiation in the high-gain regime exhibits exponential growth and guiding, and is fully coherent transversely. An undulator with N about 1000 in a bypass of a low-emittance storage ring can generate tens of megawatts of peak coherent power at wavelengths shorter than 1000 Å [7]. These are the subjects of Section 4.

2. Brightness, Flux, and Coherence

(a) Quantities Characterizing Radiation Sources

In discussing the propagation properties of radiation, the density of the photon flux in phase space plays a fundamental role and is generally referred to in optics as the brightness [8,9]. The brightness is the phase-space density of the photon flux, evaluated in the forward direction and at the center of the source, i.e., at the origin of the phase space, as follows:

$$\mathscr{B} = \frac{d^4\mathscr{F}}{d\theta d\psi dx dy}_0 . \tag{1}$$

Here θ and ψ are the horizontal and vertical angles, and x and y are the horizontal and vertical coordinates, respectively. (It should be noted that this quantity is sometimes called the brilliance.) The brightness uniquely characterizes the strength of a radiation source, as it is invariant under propagation through linear optical elements, such as lenses or free space.

Integrating the phase-space density over the angles or the position coordinates, we obtain the spatial or angular density of flux:

$$\frac{d^2\mathscr{F}}{dxdy} = \int \frac{d^4\mathscr{F}}{d\theta d\psi dx dy} d\theta d\psi , \tag{2}$$

$$\frac{d^2\mathscr{F}}{d\theta d\psi} = \int \frac{d^4\mathscr{F}}{d\theta d\psi dx dy} dx dy . \tag{3}$$

For synchrotron radiation, the angular density of flux [Eq. (3)] has traditionally been the most familiar quantity, as it can be calculated from standard textbook formulas, and it is sometimes mistakenly called brightness. However, it is not an invariant measure of the source strength, because its magnitude depends on the nature of the beam line focusing element. Finally, one obtains the flux by integration, as follows:

$$\mathscr{F} = \int \frac{d^2\mathscr{F}}{d\theta d\psi} d\theta d\psi = \int \frac{d^2\mathscr{F}}{dxdy} dx dy . \tag{4}$$

The flux is another invariant that characterizes the source strength.

It is generally convenient to consider the various differential fluxes introduced above in a small bandwidth around a given energy. In this case, we use the adjective *spectral*. Thus, we speak of the spectral brightness, spectral flux, the angular density of spectral flux, and so on.

(b) Calculation of the Brightness

The calculation of the brightness is straightforward in geometric optics. For synchrotron radiation, it is obtained by the following steps:

(i) The source brightness of a single electron is given by the Wigner distribution [10] of the electric field as follows:

$$\mathscr{B}^0(\mathbf{x},\boldsymbol{\phi}) = \text{const} \int d\boldsymbol{\xi}^2 \, \mathscr{E}^*(\boldsymbol{\phi} + \boldsymbol{\xi}/2) \, \mathscr{E}(\boldsymbol{\phi} - \boldsymbol{\xi}/2) \, e^{-ik\mathbf{x}\cdot\boldsymbol{\xi}}, \tag{5}$$

where $\boldsymbol{\phi} = (\theta,\psi)$, $\mathbf{x} = (x,y)$, $k = 2\pi/\lambda$, λ = wavelength, and $\mathscr{E}$ is the angular spectrum of the electric field given by (MKS units)

$$\mathscr{E}(\boldsymbol{\phi}) = \frac{ek}{4\pi\epsilon_0 c\lambda} \int dt \; \mathbf{n} \times (\mathbf{n} \times \mathbf{v}) \, e^{i\omega(t - \mathbf{n}\cdot\mathbf{r}/c)}. \tag{6}$$

Here e = electron charge, ϵ_0 = vacuum dielectric constant, c = light velocity, $\mathbf{n} = (\boldsymbol{\phi}, 1 - \boldsymbol{\phi}^2/2)$ is the direction vector, and $\mathbf{x}$ and $\mathbf{v}$ are, respectively, the position and the velocity vector of the electron trajectory.

(ii) For N_e electrons distributed randomly, the brightness is given by

$$\mathscr{B}(\mathbf{x},\boldsymbol{\phi}) = N_e \int \mathscr{B}^0(\mathbf{x} - \mathbf{x}_e, \boldsymbol{\phi} - \boldsymbol{\phi}_e) f(\mathbf{x}_e, \boldsymbol{\phi}_e) \, d\mathbf{x}_e^2 \, d\boldsymbol{\phi}_e^2. \tag{7}$$

Here $f(\mathbf{x}_e, \boldsymbol{\phi}_e)$ is the probability distribution function of electrons. The area of the $\mathbf{x}_e - \boldsymbol{\phi}_e$ space is known as the beam emittance.

(iii) The above expression is the brightness referred to the source plane at $z = 0$, where z is the longitudinal coordinate along the optical axis. For the brightness at $z \neq 0$, one uses the following transformation rule:

$$\mathscr{B}(\mathbf{x},\boldsymbol{\phi},z_2) = \mathscr{B}(\mathbf{x}',\boldsymbol{\phi}',z_1), \quad \begin{pmatrix} \mathbf{x}' \\ \boldsymbol{\phi}' \end{pmatrix} = M^{-1} \begin{pmatrix} \mathbf{x} \\ \boldsymbol{\phi} \end{pmatrix}. \tag{8}$$

Here M is a 2×2 matrix given by a product of matrices—one for each lens and free space. These matrices are given by

$$M_\ell = \begin{pmatrix} 1 & \ell \\ 0 & 1 \end{pmatrix} \qquad \text{for a free space of length } \ell,$$

$$M_f = \begin{pmatrix} 1 & 0 \\ -1/f & 1 \end{pmatrix} \quad \text{for a lens of focal length } f. \tag{9}$$

Once the brightness is determined, other quantities of physical interest are obtained by integration, Eqs. (2)–(4).

The method summarized here is a systematic approach for the calculation of the intensity distribution at an arbitrary transverse plane, taking into account the effects of electron-beam emittance, finite distance from source, and diffraction. An alternative method would be to evaluate the full radiation formula, keeping all the near-field terms. The latter method involves complicated numerical integrations which must be repeated from the beginning for intensity calculations at different z with the same source.

(c) Coherence

Another important characteristic of the photon beam is the coherence, which is the degree to which the radiation can exhibit interference patterns [11]. Two types of coherence can be distinguished [12]: The transverse coherence refers to the coherence of the electromagnetic disturbances at two points perpendicular to the propagation direction. The longitudinal (or temporal) coherence refers to the case of two points along the propagation direction.

Photons within the coherent phase-space area $\lambda/2$, where λ is the radiation wavelength, is transversely coherent. Since there are two transverse dimensions, the transversely coherent flux is given by

$$\mathcal{F}_{coh,T} = \mathcal{B}\,(\lambda/2)^2 . \tag{10}$$

The temporal coherence is characterized by the coherence length ℓ_c, which is related to the bandwidth $\Delta\lambda/\lambda$ by

$$\ell_c = \lambda(\lambda/\Delta\lambda) = \lambda^2/\Delta\lambda . \tag{11}$$

(d) Units

We choose the following units for the spectral flux and the brightness:

$$\mathcal{F} = \frac{\text{Number of photons}}{\text{(sec) (0.1\% bandwidth)}} ,$$

$$\mathcal{B} = \frac{\text{Number of photons}}{\text{(sec) (mm}^2\text{) (mrad}^2\text{) (0.1\% bandwidth)}} .$$

The coherence will be characterized by the coherent power P_{coh} which is defined to be the portion of the total power that is transversely coherent and that has a coherence length of 1 micron. With the above units, this becomes

$$P_{coh}\,[\text{watts}] = 7.63 \times 10^{-23} \times \mathcal{B}/\epsilon^2\,[\text{keV}] ,$$

where ϵ is the photon energy.

3. Characteristics of Synchrotron Radiation

The phase-space pattern of the synchrotron radiation is determined by calculating the brightness following the steps summarized in Section 2(b). In doing so, the electron distribution $f(\mathbf{x}_e,\boldsymbol{\phi}_e)$ is assumed to be Gaussian shape. The rms beam sizes in the x and y directions are respectively denoted as σ_x and σ_y. Correspondingly, the rms angular divergences are $\sigma_{x'}$ and $\sigma_{y'}$. The products

$$\epsilon_x = \sigma_x \sigma_{x'} \, , \; \epsilon_y = \sigma_y \sigma_{y'}$$

are known as the emittances of the electron beam.

(a) Undulators

The exact expression for the single-electron brightness $\mathscr{B}^0$ for undulators is rather complicated. However, one can approximate its shape by a Gaussian function. The rms angular divergence and radiation size for $\mathscr{B}^0$ are given respectively by

$$\sigma_{r'} = \sqrt{\lambda/L} \; , \sigma_r = (1/4\pi)\sqrt{\lambda L} \; . \tag{12}$$

Here L is the length of the undulator. The expression for $\sigma_{r'}$ was determined by Krinsky [3]. The expression for σ_r is obtained from the requirement that

$$\text{coherent phase-space area} = 2\pi\sigma_r\sigma_{r'} = \lambda/2 \; . \tag{13}$$

The following discussion is based on these approximations.

The pattern of undulator radiation is illustrated in Fig. 1. The spectrum is sharply peaked around odd harmonics of the fundamental photon energy given by

$$\epsilon_1 \, [\text{keV}] = 0.95 \, \frac{E^2[\text{GeV}]}{\lambda_u \, [\text{cm}] \, (1 + K^2/2)} \; . \tag{14}$$

Here, E is the electron energy, λ_u is the undulator magnet period, and K is the dimensionless deflection parameter given by

$$K = 0.934 \, B_0 \, [\text{T}] \, \lambda_u \, [\text{cm}] \, , \tag{15}$$

where B_0 is the peak magnetic field.

At each harmonic, the angular distribution has a sharp central cone, which contains most of the useful flux, together with outer rings. The rms angular size of the central cone, $\sigma_{Tx'}$ (or $\sigma_{Ty'}$) in the x (or y) direction, is given by a Gaussian sum of the diffraction-limited angular cone $\sigma_{r'}$ and the electron beam angular divergence $\sigma_{x'}$ (or $\sigma_{y'}$):

$$\sigma_{Tx'} = \sqrt{\sigma_{x'}^2 + \sigma_{r'}^2} \, ,$$

$$\sigma_{Ty'} = \sqrt{\sigma_{y'}^2 + \sigma_{r'}^2} \, . \tag{16}$$

The effective source size is given in each direction by a Gaussian sum of the diffraction-limited source size σ_r and the electron beam size as follows [13]:

$$\sigma_{Tx} = \sqrt{\sigma_x^2 + \sigma_r^2} \, ,$$

$$\sigma_{rT} = \sqrt{\sigma_r^2 + \sigma_r'^2} . \tag{17}$$

This will be the size of the image when the undulator radiation is focused through one-to-one optics.

The spectral flux contained in the central cone at the nth harmonic, within a 0.1% bandwidth, is given approximately by

$$\mathcal{F}_n = 1.43 \times 10^{14} N Q_n(K) I[A] , \tag{18}$$

where N is the number of undulator periods, I is the beam current, and Q_n is given as

$$Q_n(K) = \frac{nK^2}{(1 + K^2/2)} \left\{ J_{\frac{n-1}{2}} \left[\frac{nK^2}{4(1 + K^2/2)} \right] - J_{\frac{n+1}{2}} \left[\frac{nK^2}{4(1 + K^2/2)} \right] \right\}^2 , \tag{19}$$

where the J's are Bessel functions. The flux densities can now be obtained by dividing Eq. (18) by an appropriate source or angular area. In particular, the spectral brightness is given by

$$\mathcal{B}_n = \frac{\mathcal{F}_n}{(2\pi)^2 \sigma_{Tx} \sigma_{Ty} \sigma_{Tx'} \sigma_{Ty'}} . \tag{20}$$

The phase-space area defined by the central cone ($\sigma_{Tx'}$, $\sigma_{Ty'}$) and the effective source size (σ_{Tx}, σ_{Ty}) is larger than the diffraction-limited phase-space area $\lambda/2$ due to the electron beam emittance. If the emittances are such that

$$\epsilon_x, \epsilon_y \lesssim \lambda/4\pi , \tag{21}$$

then the undulator radiation will be essentially coherent transversely. Such is the case for undulator radiation from next-generation storage rings in the VUV and soft x-ray regions.

The natural bandwidth of undulator radiation at the nth harmonic is $\Delta\lambda/\lambda \cong nN$; thus, the coherence length is given by

$$\ell_c = nN\lambda ,$$

which corresponds to the relativistically contracted length of the undulator.

(b) Wigglers and Bending Magnets

Wigglers are distinguished from undulators both by a large value of K and by a high harmonic number n. The spectral peaks of wiggler radiation from neighboring harmonics smear out because of electron-beam emittance effects, and the spectral and angular distributions of the radiation become similar to those of bending magnets, except for a $2N$-fold increase in intensity. The spectrum peaks around the critical energy, which is given by $\epsilon_c[\text{keV}] = 0.665 E^2[\text{GeV}] B[\text{T}]$, beyond which it decreases exponentially.

The pattern of wiggler or bending-magnet radiation is illustrated in Fig. 2. The angular density (per milliradian) of spectral flux from a bending magnet in the forward direction, within a 0.1% bandwidth, is given by

$$\left.\frac{d^2\mathcal{F}}{d\theta d\psi}\right|_{\psi=0} = 1.327 \times 10^{13} E^2[\mathrm{GeV}] I[A] \zeta^2 K_{2/3}^2(\zeta/2) , \tag{21}$$

where K is a modified Bessel function of the second kind and ζ is the photon energy in units of the critical energy. For wigglers the fluxes should be multiplied by an additional factor $2N$. The distribution, integrated over the vertical angle ψ, is

$$\frac{d\mathcal{F}}{d\theta} = 2.46 \times 10^{13} E[\mathrm{GeV}] I[A] \zeta \int_{\zeta}^{\infty} K_{5/3}(\zeta') d\zeta' . \tag{22}$$

For bending magnets, the angular distribution is independent of the horizontal angle θ, whereas it extends to an angle δ for wigglers, where $\delta = K/\gamma$. Here, $\gamma = E[\mathrm{GeV}] \times 10^3/0.511$.

For wigglers and bending magnets, the radiation is emitted mainly in the direction parallel to the instantaneous motion of the electron. Assuming that photons from different point of the trajectory are incoherent, the brightness due to a single electron is [4]

$$\mathcal{B}^0(\theta,\psi,x,y) = \frac{d^2\mathcal{F}^0}{d\theta d\psi} \sum \delta[x - \bar{x}(\theta) + \theta\bar{y}(\theta)]\, \delta[y + \psi\bar{y}(\theta)] . \tag{23}$$

Here $d^2\mathcal{F}^0/d\theta d\psi$ is the angular density of the flux for a single electron, and $\bar{x}(\theta)$ and $y(\theta)$ are the coordinates of the point on the trajectory at which the slope is θ. There are, in general, a multiplicity of such points. The summation in Eq. (23) is over those points.

The function $d^2\mathcal{F}^0/d\theta d\psi$ will be assumed to be uniform in θ. In the vertical direction (ψ direction), it is approximated by a Gaussian shape with the rms angular divergence given by

$$\sigma_\psi = \frac{1}{\sqrt{2\pi}} \frac{d\mathcal{F}}{d\theta} \Big/ \left.\frac{d^2\mathcal{F}}{d\theta d\psi}\right|_{\psi=0} . \tag{24}$$

At the critical energy, this becomes $0.32/\gamma$ [13]. The diffraction-limited source size σ_r associated with σ_ψ can be computed from the coherence requirement [Eq. (13)]:

$$\sigma_r = \lambda/4\pi\sigma_\psi . \tag{25}$$

For consistency, we replace the delta functions in Eq. (23) by

$$\delta(x) \rightarrow \frac{1}{\sqrt{2\pi}\,\sigma_r} \exp\left(-\frac{1}{2}\frac{x^2}{\sigma_r^2}\right) . \tag{26}$$

The brightness for the electron beam can then be computed using Eq. (7). To simplify the calculation, we neglect the effect of the curvature of the electron trajectory on the effective source size. The expression for the bending-magnet brightness then becomes

$$\mathscr{B} = \frac{d^2\mathscr{F}}{d\theta d\psi}\Big|_0 \Big/ 2\pi \left[(\sigma_x^2 + D^2\sigma_\epsilon^2 + \sigma_r^2) \left(\sigma_y^2 + \sigma_r^2 + \frac{\epsilon_y^2 + \gamma_y \sigma_r^2}{\sigma_\psi^2} \right) \right]^{1/2} . \tag{27}$$

In the above, γ_y is the third betatron function in the y direction, ϵ_y is the beam emittance, D is the dispersion function in the x direction, and σ_ϵ is the rms value of the relative energy spread. Notice that the nonvanishing dispersion function in the bending magnet contributes to an additional term in the effective source size, proportional to the energy spread.

The brightness expression for wigglers is

$$\mathscr{B} = \frac{d^2\mathscr{F}}{d\theta d\psi} \sum_{\pm n,\left|-\frac{N}{2}\right|}^{\left|\frac{N}{2}\right|} \frac{1}{2\pi} \frac{\exp\left[-\frac{1}{2} \left(\frac{x_0^2}{\sigma_x^2 + z_{n\pm}^2 \sigma_{x'}^2} \right) \right]}{\left[(\sigma_x^2 + z_{n\pm}^2 \sigma_{x'}^2) \left(\frac{\epsilon_y^2}{\sigma_\psi^2} + \sigma_y^2 + z_{n\pm}^2 \sigma_{y'}^2 \right) \right]^{1/2}} ,$$

$$z_{n\pm} = \lambda_w \left(n \pm \frac{1}{4} \right) . \tag{28}$$

Here λ_w is the wiggler period. The effects of the depth of field — a result of the contributions from different poles — are apparent in the above expression. The exponential factor in Eq. (28) arises from the fact that wigglers have two source points, separated by $2x_0$, where

$$x_0 = \frac{K}{\gamma} \frac{\lambda_w}{2\pi} . \tag{29}$$

(c) Undulators and Wigglers for the Proposed Light Source at Berkeley

There are several proposals for next-generation synchrotron radiation facilities [14]. These are all based on low-emittance (less than 10^{-8} m-rad), high-current (several hundred milliamperes) electron or positron storage rings, and are optimized for undulator operation to produce high-brightness radiation. Of these the 5–7 GeV machines are optimum for hard x-rays, and the 1–2 GeV machines for the VUV and the soft x-ray spectral regions. Here we describe the undulators and wigglers and their performances for one of the latter

machines, the 1.5-GeV Light Source proposed by Lawrence Berkeley Laboratory [15].

The electron parameters of the Light Source relevant to our discussion here are electron energy = 1.5 GeV, beam current (average) = 400 mA, $\epsilon_x = 4 \times 10^{-9}$ m-rad, and $\epsilon_y = 0.1 \times \epsilon_x$. Table 1 summarizes the parameters for four possible undulators and a wiggler. These parameters are chosen so that the spectrum covers the VUV and the soft x-ray regions in an orderly and overlapping fashion. The devices also provide some coverage down to 0.5 eV in the near-infrared region (by means of the undulator U20.0) and up to about 10 keV in the hard x-ray region (by means of the wiggler W13.6).

The spectral flux and the spectral brightness for these devices are shown in Figs. 3 and 4, respectively. Figure 5 gives the coherent power as defined in Section 2(d).

For undulators we take the view that the first and third harmonics provide useful output (harmonics of higher order are also present, but they are less useful and also more sensitive to construction errors). This point is important, because it is generally possible to design beam line optical systems to handle wider energy ranges than can be covered with the fundamental radiation of an undulator. As a rough guide, the useful operating range of an undulator is considered to lie between the energy of the fundamental at the largest achievable K value and the energy of the third harmonic at $K = 0.5$. It is on this basis that the working ranges of the specified devices are said to overlap.

For a given total length of undulator and for a given desired photon energy, it is usually better to choose a higher value of K. This is because the spectral flux in the central cone [see Eq. (18)] is proportional to $Q_n(K)$, which increases with K. In addition, the larger K also implies a shorter period length [see Eq. (14)], hence a further increase in flux by virtue of the larger number of periods, N. However, the validity of this rule is limited by power considerations: As the value of K becomes large, the undulator effectively becomes a wiggler for large harmonic numbers n, and the total power generated, most of which is in unwanted spectral regions, may become unacceptably large. For each insertion device listed in Table 1, the total power is limited to a few kilowatts.

Higher photon energies are generally obtained by using a shorter period length; however, there is a lower limit to the practical period length of an undulator, because the magnetic field decreases rapidly as the ratio of the period length to the magnet gap becomes small. The magnets are of the hybrid configuration, consisting of steel poles and permanent magnets [16]. The minimum magnet gap is assumed to be 1.5 cm.

4. From Undulators to High-Gain Free Electron Lasers

In simple undulators discussed so far, electrons, which are initially uncorrelated, remain essentially uncorrelated as the electron bunch moves through the undulator. The radiation emitted in this case, called the undulator radiation, is analogous to the spontaneous emission in atomic systems. As the number of the undulator periods, N, increases, the cumulative effects of the radiation–electron beam interaction could lead to a density modulation in the electron beam and an exponential amplification of the undulator radiation. Undulators operating in this regime will be called the high-gain FELs. The radiation emitted in this case will be called self-amplified spontaneous emission (SASE) by analogy with laser terminology.

The high-gain FELs operating in the SASE mode do not require the use of high-reflectivity mirrors to form optical cavities. Thus, they are promising alternatives to the

usual FELs as generators of intense, coherent radiation at wavelengths shorter than 1000 Å. At microwave wavelengths, the principle of SASE has been experimentally confirmed at Lawrence Livermore National Laboratory [17].

(a) Characteristics

The radiation characteristics of high-gain FELs have been studied with various degrees of sophistication [2,5,18–21]. Here, we summarize the results of the recent analysis based on the three-dimensional Maxwell-Klimontovich equations [5].

An important parameter characterizing high-gain FELs is the following dimensionless quantity [2]:

$$\rho = \left[\frac{e\ j\ K^2 |JJ|^2\ \lambda_u^2}{32\ (2\pi)^2\ \gamma_o^3\ mc^3\ \epsilon_0} \right]^{1/3}$$

where j is the beam current density and $|JJ|$ is the Bessel function factor in the curly brackets in Eq. (19). For cases considered here, ρ is typically of order 10^{-3}.

Figure 6 summarizes the evolution of radiation characteristics from simple undulators to SASE. For $\rho N \ll 1$, the radiation is an incoherent superposition of radiation from individual electrons and is referred to as undulator radiation. It is partially coherent transversely due to finite electron beam emittances. The bandwidth is about $1/N$. For larger N but with $\rho N \lesssim 1$, the FEL interaction causes modulation in the correlation of the electrons, resulting in enhanced radiation intensity and coherence. Barring certain degenerate situations, the radiation amplitude is dominated by a single mode which grows exponentially is fully coherent transversely. The relative bandwidth in this exponentially growing regime is smaller than that of the undulator radiation by a factor $\sqrt{\rho N}$. Finally, the exponential growth stops when $\rho N \sim 1$ due to the increased momentum spread induced by the FEL interaction.

High-gain FELs can also be used in an amplifier mode if coherent input radiation is available at the desired wavelengths. The coherence properties of the emitted radiation in this mode would be the same as those of the input.

(b) A High-Gain FEL in a Bypass of a Storage Ring

Modern storage rings provide the high-density electron beams required for high-gain FEL operation. For efficient interaction, the undulator must be long and have a narrow gap. Such a device, if placed in a normal section of a storage ring, would severely limit the acceptance of the ring and thus reduce the beam lifetime due to scattering with the residual gas. Moreover, the interaction of the beam with an FEL undulator is disruptive to the beam itself in terms of energy loss and increased momentum spread. To avoid these problems, the undulator can be placed in a special bypass section [7], as shown schematically in Fig. 7. The electron beam normally circulates in the storage ring without passing through the FEL undulator. Once every damping time, the beam is directed into the bypass section, where the interaction with the undulator takes place, generating intense, coherent radiation. As the beam leaves the undulator, it is deflected back into the storage ring, where synchrotron radiation damping reduces the induced energy spread. After one damping time, the

beam is ready to be injected into the bypass again.

A feasibility study of an optimized storage ring for a high gain FEL operating at 400 Å was recently carried out at Lawrence Berkeley Laboratory [22,23]. Important aspects of storage ring issues, such as collective instabilities and lattice optimization, bypass considerations, and operational requirements were studied. By studying several examples of 750-MeV storage ring lattices, it was concluded that the high beam quality demanded for these high-gain FELs can be achieved with presently available accelerator technology.

The storage ring for the Light Source discussed in Section 3(c) is not optimized for high-gain FELs, but could still provide significant performance when the beam energy is lowered to 750-MeV. Table 2 gives the electron beam parameters for 750-MeV operation and possible undulator parameters for 400 Å radiation [24]. The expected amplification factors (for the amplifier mode) and the SASE power is shown for different undulator lengths in Table 3. The laser saturates for a 45-m undulator, and generates 10 MW of SASE power. However, the maximum length of the undulator in a bypass that can be fitted inside the storage ring is 20 m, which the SASE power is only 0.8 kW. To reach saturation in a 20-m undulator, we can install two low-reflectivity mirrors at each end of the undulator, and run the storage ring with a few electron bunches separated by twice the distance between mirrors. Mirrors at these wavelengths could be made from multilayer materials. Assuming a 30% reflectivity, saturated laser operation is possible with three bunches stored in the ring.

References

[1] D.T. Attwood and K-J. Kim, Nucl. Instr. and Meth., A246 (1986) 86.
[2] B. Bonifacio, N. Narducci and C. Pellegrini, Opt. Comm. 50 (1984) 373.
[3] See for example, S. Krinsky, IEEE Trans. Nucl. Sci. NS-30 (1983) 3078.
[4] K-J. Kim, Nucl. Instr. and Meth. A246 (1986) 71; SPIE proceedings, Vol. 582, p. 2.
[5] R. Coïsson and R.P. Walker, SPIE proceedings, Vol. 582, p. 24.
[6] K-J. Kim, Phys. Rev. Lett. 57 (1986) 1871.
[7] J. Murphy and C. Pellegrini, J. Opt. Soc. Am. *1B* (1984) 530.
[8] M. Born and E. Wolf, Principle of Optics, 6th ed. (Pergamon Press, Oxford, New York, 1980). Chapter 4.
[9] G.K. Green, Spectra and Optics of Synchrotron Radiation (1976) BNL 50522.
[10] E. Wigner, Phys. Rev. 40 (1932) 749.
[11] M. Born and E. Wolf, ibid., Chapter 10.
[12] See for example, J.W. Goodman, Statistical Optics (John Wiley and Sons, New York, 1985) Chapter 5.
[13] This differs from Ref. [9] due to different ways of defining the rms values.
[14] See for example, H. Winick, Status of Synchrotron Radiation Facilities outside the USSR, these Proceedings.
[15] Lawrence Berkeley Laboratory Report, 1–2 GeV Synchrotron Radiation Source (1986) Pub-5172 Rev.
[16] K. Halbach, J. Phys. (Paris) 44 (1983) C1-211.
[17] T.J. Orzechowski et al., Phys. Rev. Lett. 54 (1985) 889.
[18] K-J. Kim, Nucl. Instr. and Meth. A250 (1986) 396.
[19] J-M. Wang and L-H. Yu, Nucl. Instr. and Meth. A250 (1986) 484.
[20] K-J. Kim and C. Pellegrini, Amer. Inst. Phys. Conference Proceedings, No. 147 (1986) 17.
[21] L.H. Yu and S. Krinsky, Amer. Inst. Phys. Conference Proceedings, No. 147 (1986) 299.
[22] K-J. Kim, J.J. Bisognano, A.A. Garren, K. Halbach, and J.M. Peterson, Nucl. Instr. and Meth. A239 (1985) 54.
[23] J.J. Bisognano et al., Particle Accelerators, 18 (1986) 223.
[24] The numbers are computed by M. Zisman.

Table 1. Parameters for the possible insertion devices and the bending magnets chosen for the LBL 1–2 GeV Light Source.

Name	Period (cm)	No. of periods	Photon energy range (eV)[a]	Critical energy (keV)
Undulators				
U20.0	20.0	23	0.5–95 |1.5–285|	–
U9.0	9.0	53	5–211 |15–633|	–
U5.0	5.0	98	50–380 |150–1140|	–
U3.65	3.65	134	183–550 |550–1650|	–
Wiggler				
W13.6	13.6	16	–	3.1
Bending magnet	–	–	–	1.9

[a]The photon energy range of the fundamental and the third harmonic (shown in brackets) as K decreases from its maximum value to 0.5.

Table 2. Electron-beam and undulator parameters for a 400 Å high-gain FEL.

Electron energy	750 MeV
Horizontal emittance	3.5×10^{-9} m-rad
Vertical emittance	3.5×10^{-10} m-rad
Peak current	20 A
Momentum spread	0.1%
Undulator period	2.34 cm
K (peak)	3.65
Magnet gap	3.5 cm
ρ	8.8×10^{-4}

Table 3. Performance of a high-gain FEL operating in a storage ring with the parameters of the LBL Light Source.

Length of the Undulator	Amplification	SASE Power
20 m	1300	0.8 kW
25 m	8000	5.0 kW
45 m	10^7	10.0 MW

Figure Captions

Fig. 1. The angular-spatial pattern of undulator radiation.

Fig. 2. The angular pattern of radiation from wigglers and bending magnets.

Fig. 3. The spectral flux from the proposed LBL Light Source [15]. For undulators, solid lines represent the fundamental and dashed lines the third-harmonic radiation. For wigglers and bending magnets, a 5 mrad horizontal collection angle is assumed.

Fig. 4. The spectral brightness from the proposed LBL Light Source [15]. For undulators, solid lines represent the fundamental and the dashed lines third-harmonic radiation.

Fig. 5. The average coherent power from the undulators for the proposed LBL Light Source [15]. The dashed line third-harmonic radiation.

Fig. 6. A schematic representation of SASE as a function of the number of undulator periods, N.

Fig. 7. A schematic illustration of high-gain FEL operation in the bypass of a storage ring.

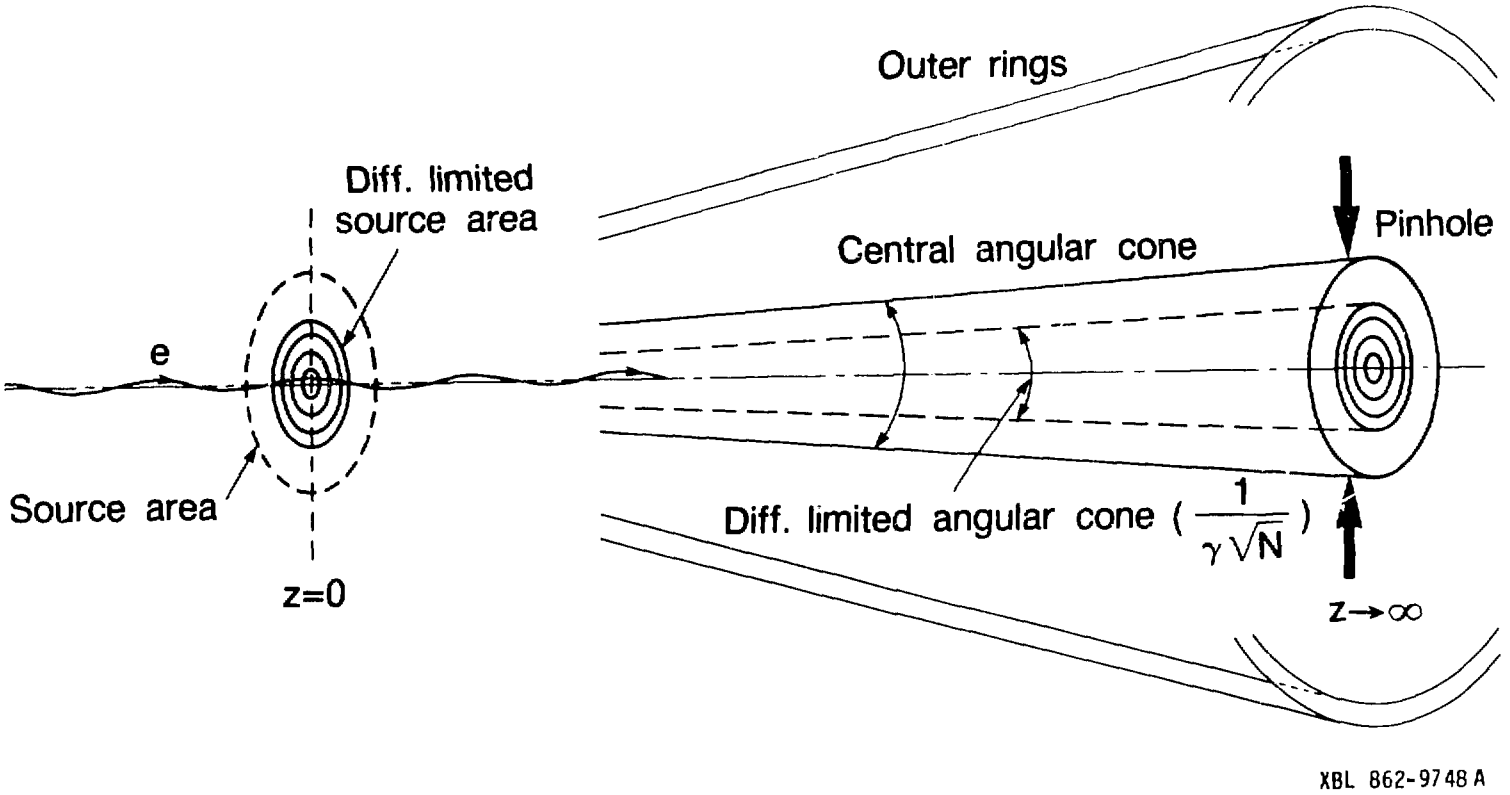
Outer rings
Diff. limited
source area
Central angular cone
Pinhole
e
Source area
z=0
Diff. limited angular cone ($\frac{1}{\gamma\sqrt{N}}$)
z→∞
XBL 862-9748 A

Fig. 1

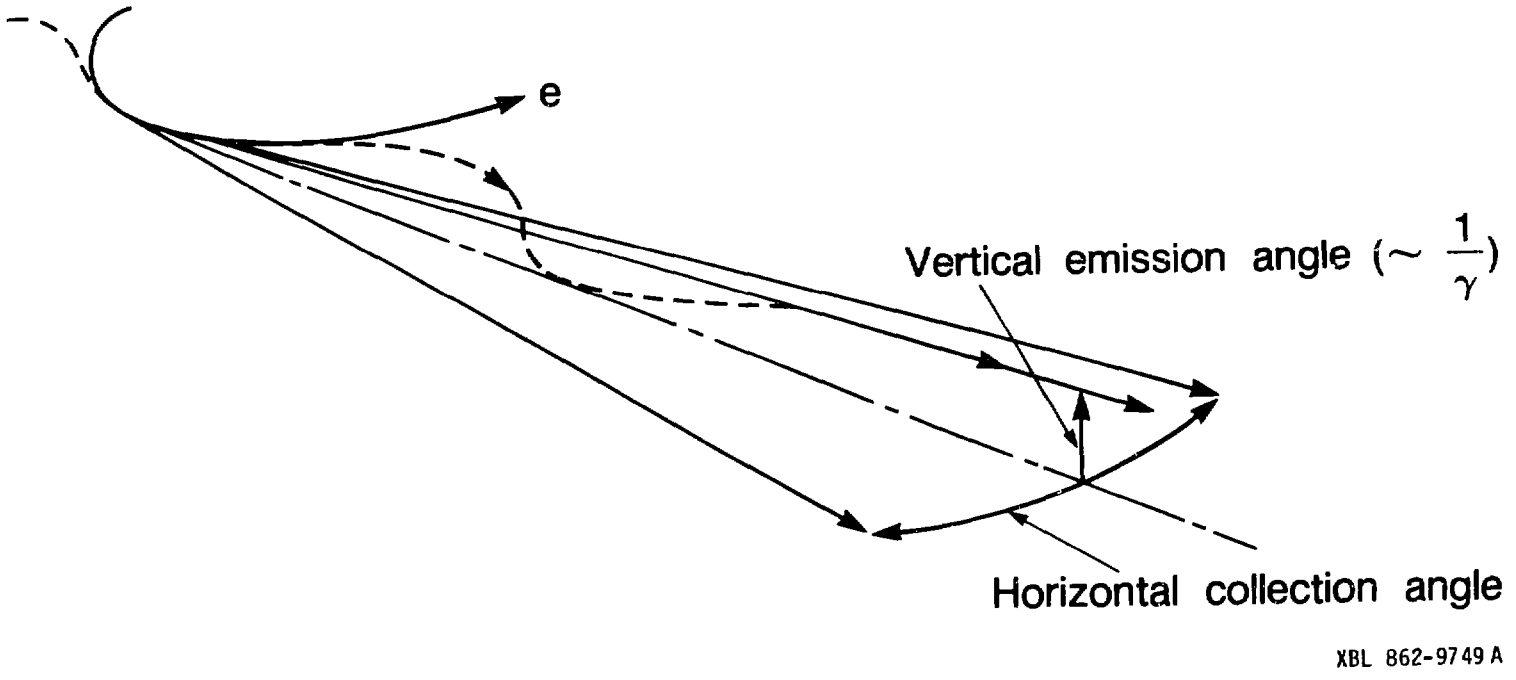
e
Vertical emission angle (~ 1/γ)
Horizontal collection angle
XBL 862-9749 A

Fig. 2

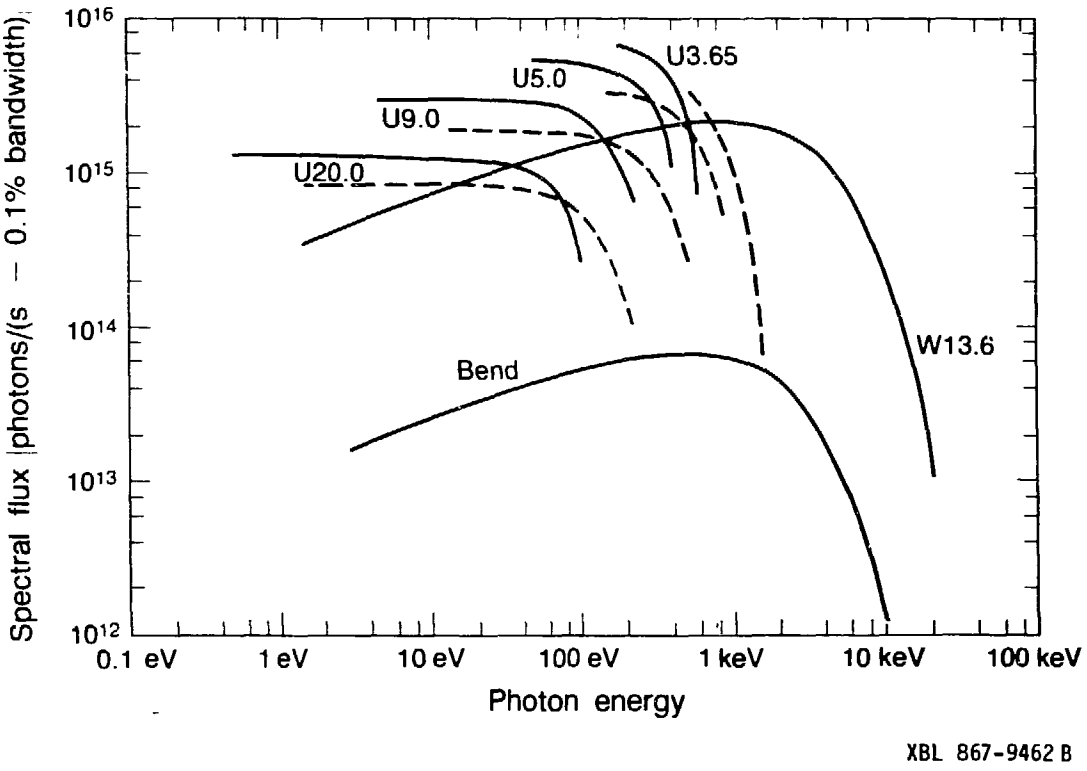
Spectral flux (photons/(s − 0.1% bandwidth))
10^16
10^15
10^14
10^13
10^12
U3.65
U5.0
U9.0
U20.0
W13.6
Bend
0.1 eV
1 eV
10 eV
100 eV
1 keV
10 keV
100 keV
Photon energy
XBL 867-9462 B

Fig. 3

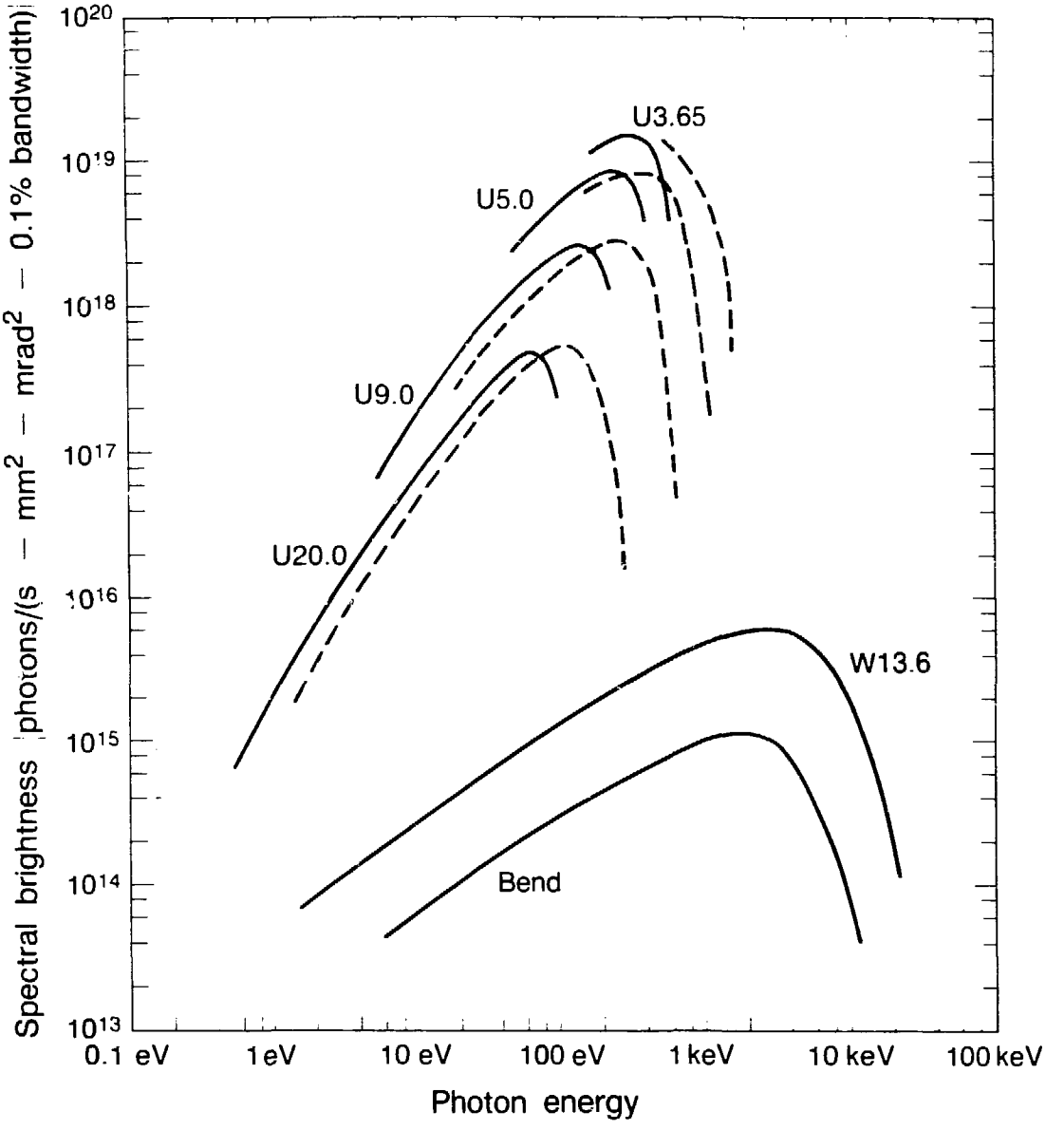
Spectral brightness (photons/(s — mm² — mrad² — 0.1% bandwidth))
10²⁰
10¹⁹
10¹⁸
10¹⁷
10¹⁶
10¹⁵
10¹⁴
10¹³
U3.65
U5.0
U9.0
U20.0
W13.6
Bend
0.1 eV
1 eV
10 eV
100 eV
1 keV
10 keV
100 keV
Photon energy
XBL 867-9461 B

Fig. 4

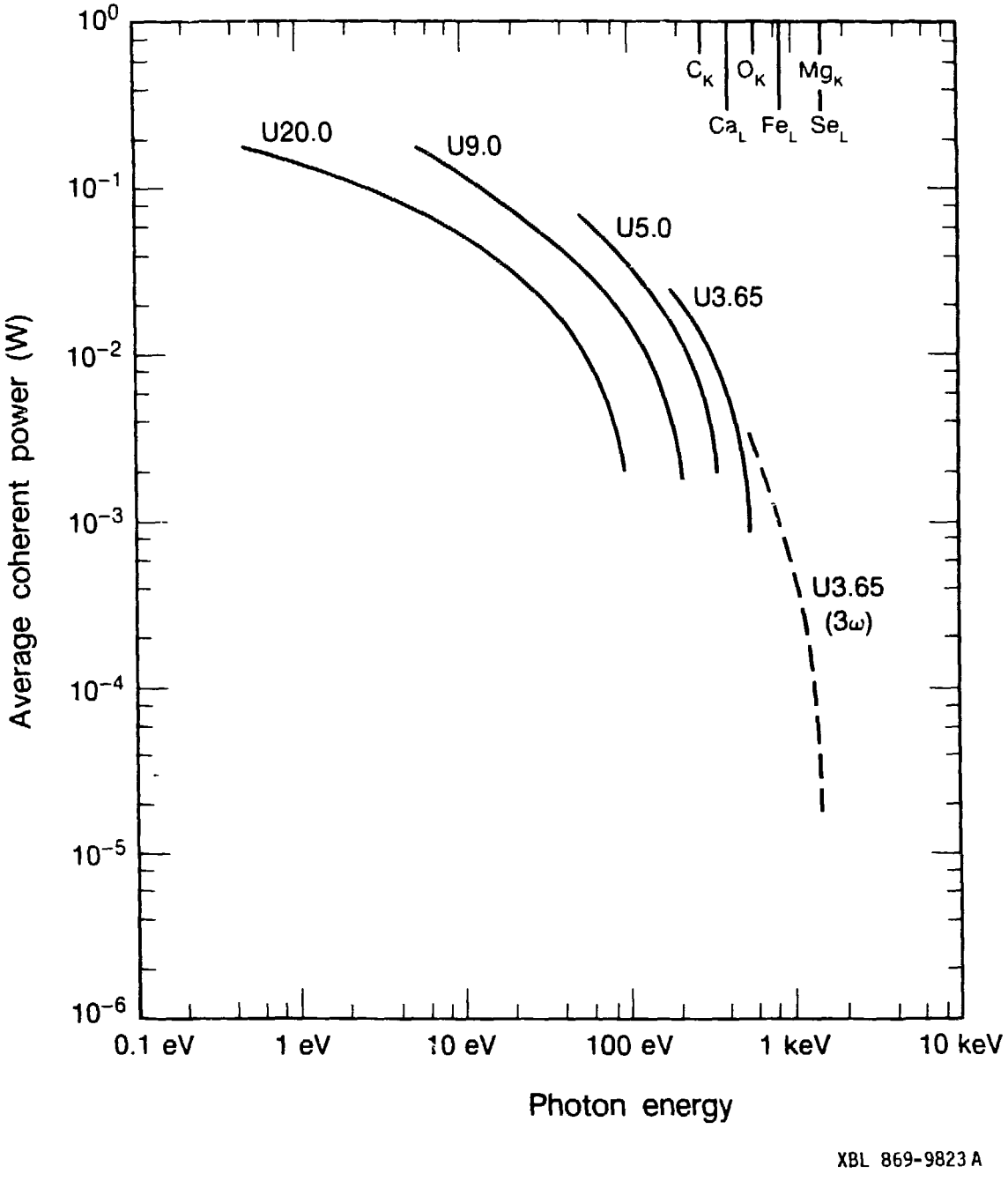
10^0
10^{-1}
10^{-2}
10^{-3}
10^{-4}
10^{-5}
10^{-6}
Average coherent power (W)
C_K O_K Mg_K
Ca_L Fe_L Se_L
U20.0
U9.0
U5.0
U3.65
U3.65
(3ω)
0.1 eV
1 eV
10 eV
100 eV
1 keV
10 keV
Photon energy
XBL 869-9823 A

Fig. 5

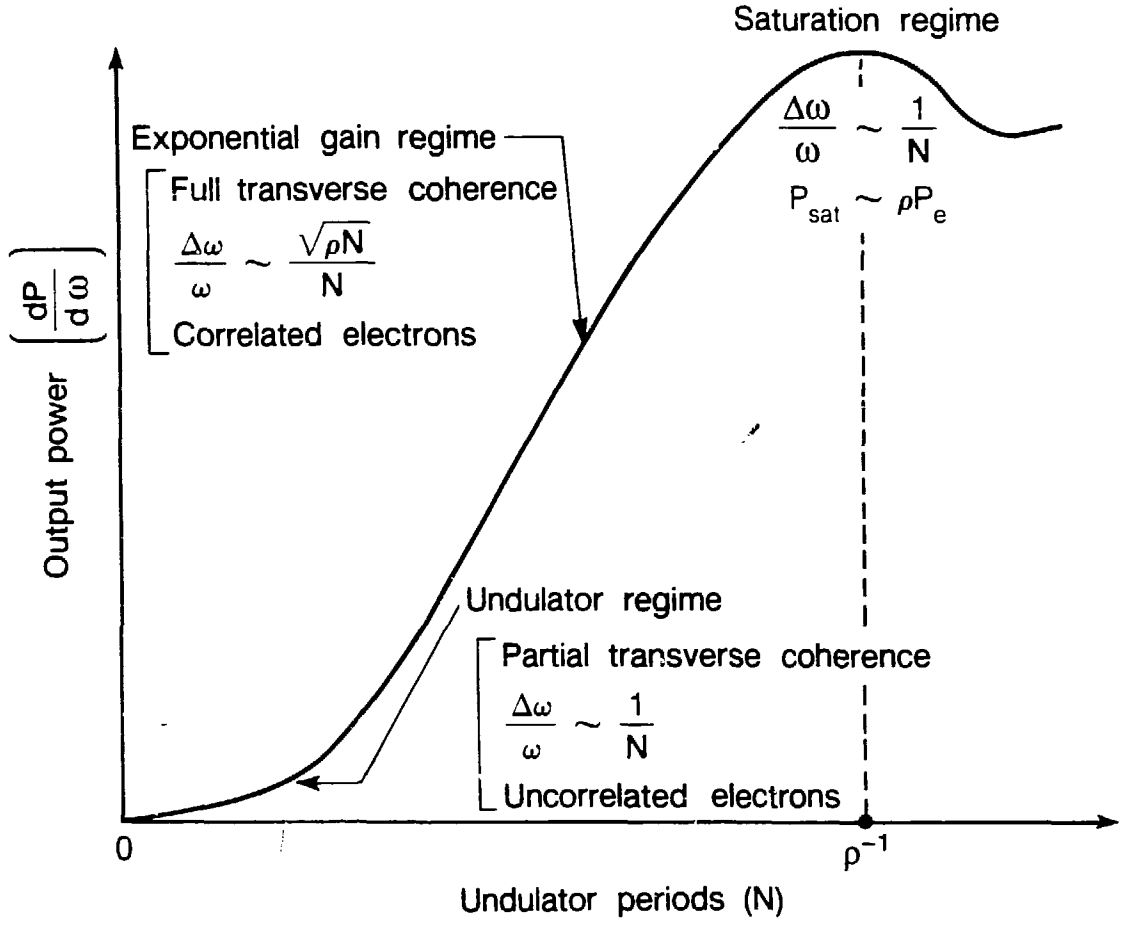
Saturation regime
Exponential gain regime
Full transverse coherence
Δω/ω ~ √ρN/N
Correlated electrons
Δω/ω ~ 1/N
P_sat ~ ρP_e
Output power (dP/dω)
Undulator regime
Partial transverse coherence
Δω/ω ~ 1/N
Uncorrelated electrons
0
ρ^-1
Undulator periods (N)
XBL 866-11164

Fig. 6

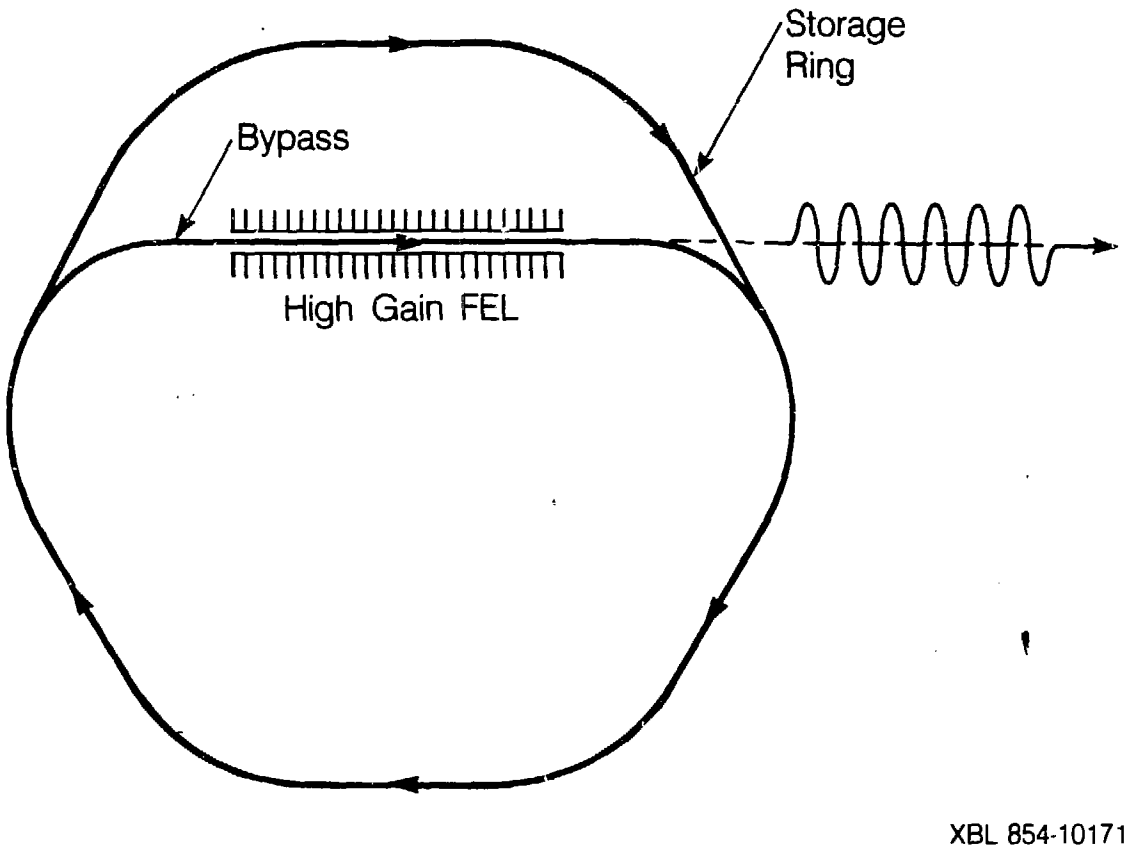

Fig. 7